Orbital dependent interaction of quantum well states for catalytic water splitting

2015 New J. Phys. 17 013023

(http://iopscience.iop.org/1367-2630/17/1/013023)

New Journal of Physics
The open access journal at the forefront of physics

Deutsche Physikalische Gesellschaft DPG
IOP Institute of Physics

Published in partnership with: Deutsche Physikalische Gesellschaft and the Institute of Physics

OPEN ACCESS

RECEIVED
21 September 2014

ACCEPTED FOR PUBLICATION
1 December 2014

PUBLISHED
15 January 2015

PAPER

Orbital dependent interaction of quantum well states for catalytic water splitting

Zijing Ding[1], **Shiwu Gao**[2] **and Sheng Meng**[1,3]

[1] Beijing National Laboratory for Condensed Matter Physics and Institute of Physics, Chinese Academy of Sciences, Beijing 100190, People's Republic of China
[2] Beijing Computational Science Research Center, Beijing 100084, People's Republic of China
[3] Collaborative Innovation Center of Quantum Matter, Beijing 100190, People's Republic of China

E-mail: smeng@iphy.ac.cn

Keywords: water splitting, quantum well states, orbital symmetry, catalysis, gold clusters

Supplementary material for this article is available online

Abstract

Orientational dependence of catalytic activity for water splitting reaction on a two-dimensional gold cluster supported on MgO/Ag(001) has been identified using first-principles calculations. Strong oscillations are found in water adsorption energy, the dissociation barrier, and the binding energy of the dissociated H atom, with two different orientational patterns. These two patterns correlate with the wavefunction symmetry of frontier orbitals of selected quantum well states (QWSs). This finding reveals a new aspect of orbital symmetry in catalytic reactions without involving changes in the shape or size of the atomic cluster, and is promising for potential applications in chemical reactions using the orbital degree of freedom of QWSs.

Gold nanoparticles on oxide supports are being used to catalyze an increasing number of reactions, including low-temperature oxidation of CO [1–3], acetylene hydrochlorination [4–6], and the water–gas shift reaction [7]. Contrary to the inert behavior of bulk gold metals, gold clusters show strong catalytic activities that depend on the sizes and shapes of the supported clusters [8–10]. The atomic structures of small gold clusters, Au_n ($3 \leqslant n \leqslant 20$), have been determined over the last decade [11]. The catalytic activity for CO oxidation [12, 13] can be attributed to their unique adsorption geometries and resultant electronic structures. It has been reported that small gold clusters on MgO thin films form two-dimensional (2D) planar structures and accommodate 2D quantum well states (QWSs), which have been resolved in scanning tunneling spectroscopy and density functional theory studies [14–16]. Recently we found that the occupation of a QWS and thus the optical responses of Au_8 supported on MgO/Ag(001) can be controlled by the thickness or doping level of the oxide films [10]. Layer-dependent coupling of water molecules with QWS has also been established on thin films of alkali metals [17]. Yet a comprehensive understanding of the catalytic activation of quantum well states has not been achieved and requires further atomistic description of the QWS interacting with molecules.

Here we report on the orbital-dependent water-splitting reactivity of QWSs for gold clusters supported on MgO/Ag(001) films. These gold clusters significantly enhance water adsorption on oxide surfaces due to electron transfer between the substrate and the cluster. In addition, strong oscillations are found in water binding energy, the dissociation barrier, and the binding energy of the dissociated hydrogen atom, yet they display two different patterns in orientational dependence. These two patterns are found to correlate closely with the wavefunction symmetry and electronic density of the frontier orbital of the selected QWS of the same gold cluster. Catalytic activities can then be engineered by tuning the thickness of oxide films or blocking active sites with external adsorbates, without changing the size and shape of the atomic cluster. The conventional wisdom [18, 19] to control catalysis by adjusting sizes, shapes, or coordination numbers of clusters is thus expanded. In addition, the 2D character of supported gold clusters makes it different from the *d*-orbital of a single metal atom interacting with ligands, whereas strong steric repulsion prohibits the presence of metastable adsorption sites and effective control. This finding reveals a new aspect of orbital symmetry in water splitting reactions and is

promising for potential applications to control catalytic reactions using the angular dependence of QWS interactions.

First-principles calculations were performed in the framework of density functional theory [20] as implemented in VASP [21]. Ground-state geometries were optimized using the projector-augmented-wave pseudopotentials [22, 23] and the Perdew–Burke–Ernzerholf [24] form of exchange-correlation functional. The substrate consists of two-monolayer (2ML) MgO thin film, in registry with three Ag(001) atomic slabs with a lattice constant of 4.09 Å taken from experiment. This imposes a compressive strain of 2.85% compared with bulk MgO or 0.24% compared with 2ML MgO free-standing thin film [25]. A large Ag (6×6) supercell is used to accommodate the Au_8 cluster and the adsorbed water molecules. The plane-wave energy cutoff is 450 eV. All atoms except those in the bottom two layers of Ag are relaxed during geometry optimization until the residue forces are smaller than 0.04 eV $Å^{-1}$. Local densities of states (LDOSs) are calculated by projecting electron density onto atomic species using a Wigner–Seitz radius. The transition states for water splitting were determined using the climbing image nudged elastic band method [26].

Small gold clusters form two-dimensional structures both in a vacuum and on MgO/Ag(001) [8–10, 16]. The Au_8 is chosen as a prototype since it is a *magic* cluster, whose stability surpasses slightly larger and smaller clusters. Water adsorption on the supported clusters prefers the periphery sites of the cluster. Figure 1(a) shows a typical configuration of a water monomer on Au_8@MgO (2ML)/Ag(001), where the oxygen sits on top of a Mg atom [10, 27] with one OH bond pointing toward the gold cluster. Other stable configurations are shown by the red dots in figure 1(b), which approximately form a ring around the cluster. For all the adsorption sites, the optimized geometric configurations are similar to those in figure 1(a) (see figure S1[4]). Because the distance between the central Au atom and the oxygen atom in water is almost constant at ~6 Å, with the longest and shortest Au–O length being 3.58 and 3.18 Å and with small variations in OH bond length (figures S2 and S3), an azimuthal angle θ is used to define the orientation of these sites relative to the symmetry axis $\boldsymbol{x}$ of the cluster as sketched in figure 1(b).

The LDOS of the gold cluster on MgO/Ag(001) is displayed in figure 1(c). It consists of a quasi-continuum *s*–*d* band between –6 and –2 eV below the Fermi level. In the band gap of MgO (–2.0~2.0 eV), it has several quantum well states, QWS1 ~ QWS4, whose wavefunctions are completely localized in the gold cluster due to the presence of the MgO band gap. These QWSs have different orbital symmetries and nodal structures; see figure 1(d). QWS1 has a d_{x^2}-orbital symmetry, whereas QWS2 has a d_{xy}-orbital symmetry. Previous analysis [16] has shown that the occupation of QWS2 leads to transfer of two electrons to the supported Au_8. As we demonstrate hereafter, the charge transfer state, QWS2, and the lowest unoccupied molecular orbital, QWS3, are mainly responsible for the water–cluster coupling and the orientational dependence of the adsorption energetics.

Figure 2 shows the angular dependency of the electron density of QWS2 (a)and the adsorption energy of a water molecule (b) on Au_8@MgO/Ag(001) in the configurations shown in figure 1(b). The electron density is taken at a distance of 4.3 Å from the center of the cluster. Water adsorption energy E_{ads} is defined as the energy difference between the combined system (E_{tot}) and the isolated gaseous water (E_{H_2O}) and substrate ($E_{Au_8@MgO/Ag(001)}$):

$$E_{ads} = E_{Au_8@MgO/Ag(001)} + E_{H_2O} - E_{tot}.$$

It varies between 0.6 ~ 0.8 eV and is much larger than that on bare MgO/Ag(001), 0.42 eV. So the gold cluster generally enhances water binding by 0.2 ~ 0.4 eV, depending on the location of the water molecule relative to the symmetry axis of the gold cluster. Water adsorption energies fall in the ideal range of 0.6–0.8 eV, all larger than the cohesive energy of bulk water (0.58 eV), enabling prompt surface wetting to promote subsequent reactions. It is also worth mentioning that water molecules bind only very weakly on top of the cluster, with a binding energy smaller than 0.14 eV [10]. So the interface of the supported cluster, i.e., the periphery sites, constitutes the most favorable sites for water adsorption.

The angular dependence of the binding energy of water is associated with the angular distribution of the electron density of QWS2 along the red circle marked in the inset (the selected edge region shown in figure S4 (see footnote 4)). The density of QWS2 shows a four-lobe symmetry (see the inset). Its wavefunction has four nodes at $\theta = 0°, 90°, 180°$, and 270°, respectively. The bonding distance between the OH and the cluster, the H–Au bond length, is ≈2.2–2.4 Å. The binding energy shows angular dependence similar to that of the charge density. The maximum adsorption energy, 0.80 eV, appears at $\theta = 54°$, which corresponds to the wavefunction maximum of QWS2. Other maxima are located at $\theta = 136°, 228°$, and 394°, respectively. The minimum of the binding energy is located at $\theta = 0°$, with $E_{ads} = 0.58$ eV, although geometrically the water molecule is closest to the apex gold atom in this configuration, whose coordination number is also the lowest (see figure 1(b)). This

[4] See Supplemental Material (stacks.iop.org/njp/17/013023/mmedia) for definition of edge zone, bond length variations, water on free Au_8, bonding mechanisms, water orbital information, etc.

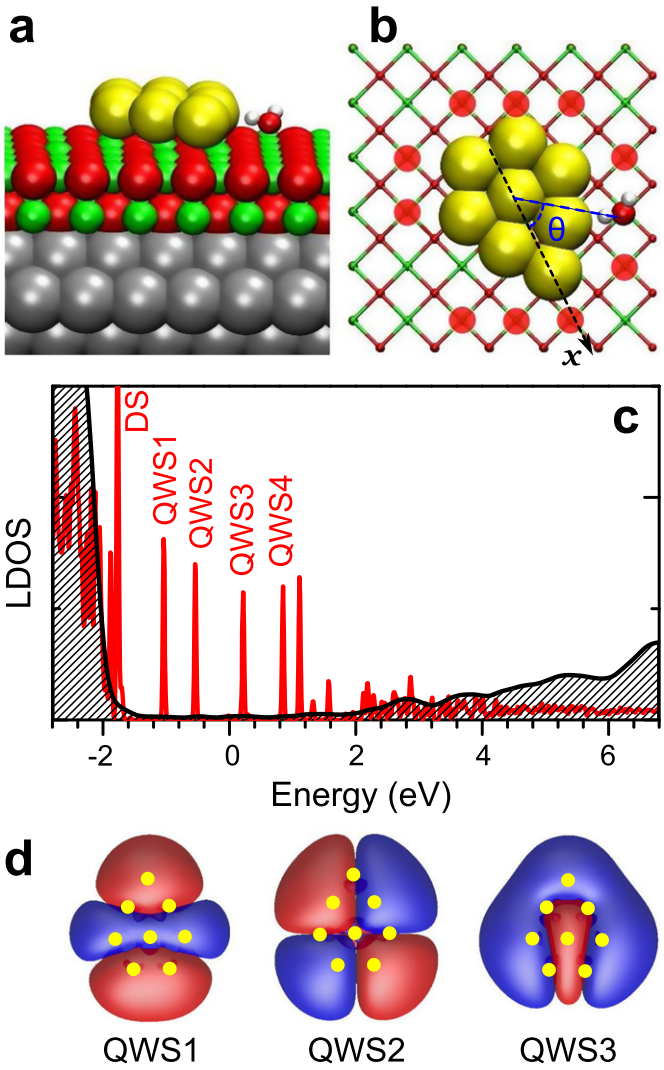

Figure 1. (a) and (b) Side and top views for one of the optimized configurations for water molecule adsorption on Au_8@MgO (2ML)/Ag(001). The green, red, yellow, white, and gray balls represent Mg, O, Au, H, and Ag atoms, respectively. The semitransparent red points denote other adsorption sites. The x-axis is the symmetry axis of the gold cluster. (c) Local density of states (LDOS) of the gold cluster (in red) and MgO (in black) for Au_8@MgO/Ag(001) with the Fermi energy level set to zero. The conduction band of the MgO film starts at ~2 eV, presenting an energy gap ~4 eV. 'DS' stands for 5d-orbital states of Au. (d) Wavefunctions of the first three quantum well states (QWSs), QWS1 ~ QWS3, computed for Au_8 in a vacuum at isosurfaces of $\pm 1.5\ \mathrm{nm}^{-\frac{3}{2}}$. The yellow balls indicate the position of the gold atoms.

indicates that the water–Au_8 interaction is governed by the global electronic structure of the QWS rather than by local atomic geometry. Other energy minima appear at $\theta = 78°, 183°$, and 253°, respectively, where the OH is directed toward the nodes of the wavefunction of the QWS2, resulting in a minimal coupling between water and QWS2. Water on a free gold cluster exhibits a similar angular dependence, showing that Mg–water bonding is not a cause of energy oscillation (see supporting information, figures S5 and S6[4]). This is also evidenced by the fact that Mg–O bond distances between the oxygen of the water molecule and the Mg atom are underneath constant, 2.11 ~ 2.14 Å, for all adsorption sites. Although the extrema of the adsorption energy deviate slightly from those of the charge density due to the discrete lattice sites of Mg, it is obvious that there is a close correlation between the charge density distribution and the water adsorption energy. This suggests that water adsorption is strongly modulated by the symmetry of the quantum well state. Strong coupling occurs when the overlap between the OH and QWS2 reaches maximum.

This conclusion is further supported by the orientation-dependent localized density of states of the water molecule in the energy range of the QWS, as shown in figure 3(a). In general, the energy and the intensity of LDOS peaks corresponding to all quantum well states change with θ. The energy shift of QWS1 is relatively small, $\leqslant$0.05 eV, indicating a much weaker coupling between water and QWS1. In contrast, both the energy and intensity of QWS2 and QWS3, which are respectively the highest occupied and lowest unoccupied orbital of supported Au_8, change more significantly. In fact, both quantities oscillate with a period of roughly 90°. This correlates well with the orbital symmetry of QWS2. Strong water binding occurs when the energy of QWS2 is

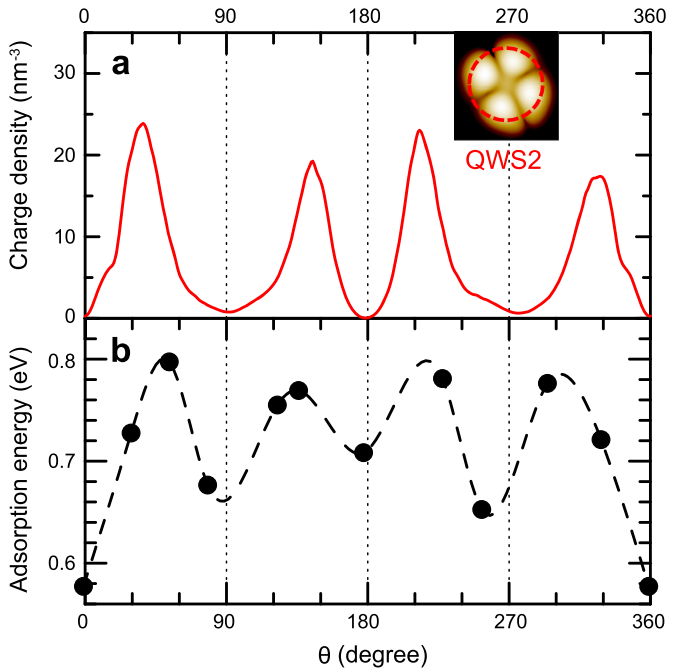

Figure 2. (a) Angular distribution of charge density of QWS2 (red line) in the selected edge region. The inset shows the shape of QWS2 and the edge zone (red circle). (b) Water adsorption energies as a function of the orientation angle of the adsorption sites shown in figure 1(b).

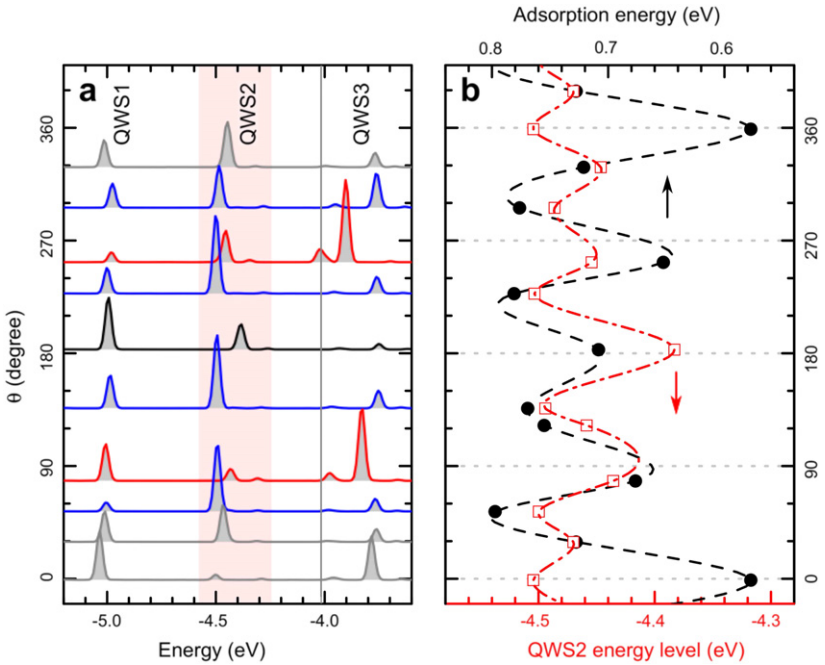

Figure 3. (a) LDOS projected onto water for water adsorption at different orientation angles θ. The vacuum energy level is set to zero. The vertical line indicates the position of the Fermi level. The blue and red curves show cases with the lowest QWS2 and QWS3, respectively. (b) The energy level of QWS2 and the water adsorption energy plotted together as a function of orientation angle θ.

mostly blueshifted and its intensity becomes largest (blue lines). Indeed, a quantitative correlation exists between the QWS2 energy level and the water adsorption energy. Both energies vary with θ following the same trend by a similar amount (except for $\theta = 0$ due to geometry asymmetry, figure 3(b)). Closer inspection shows that there is a positive linear correlation between E_{ads} and the QWS2 level for water binding at wavefunction-lobe sites, whereas an anti-correlation arises for wavefunction-node sites, with a slope of 1.00 ± 0.19 and -1.11 ± 0.29, respectively (figure 4). This means that the change in total energy of the system is simply dominated by

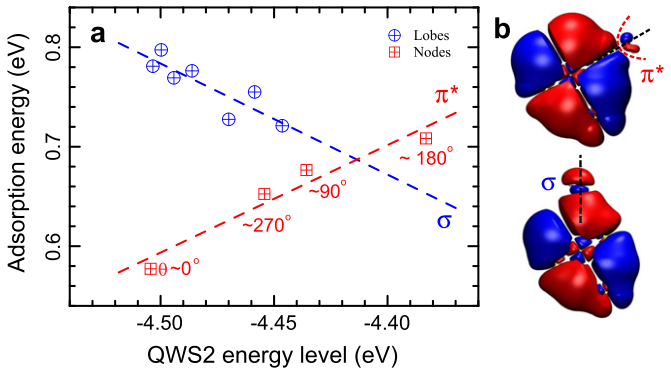

Figure 4. (a) Correlation between water adsorption energy and the QWS2 energy level for water binding at the node and lobe positions of QWS2. (b) The QWS2 wavefunction upon water adsorption shows σ and π^* bonding at the lobe and node positions, respectively.

the contribution of QWS2 electronic energy. The sign of the slope (+,−) is a result showing that water–Au_8 interaction has a bonding-like character at lobe sites and an antibonding-like character at node sites (figure 4(b)) because of the orbital symmetry of QWS2 and the orbital symmetry for unoccupied and occupied orbitals of water. (See supporting information, figures S7–S10, for discussion of bonding mechanisms[4].) Consequently a quantitative correlation between QWS2 and water reaction energy is established, where lower QWS2 upon binding interactions results in lower total energy and thus enhanced water binding by the same energy amount. The energy and intensity of QWS3 also change sensitively with θ. However, this does not contribute to the binding of the water since QWS3 is unoccupied in all configurations. From figures 2–4, we conclude that the angular dependence of water adsorption results from electronic coupling between the OH bond and the QWS2 of the supported gold cluster.

Next we study how QWSs affect the kinetic pathway and energy barrier for water dissociation. Figure 5(a) shows configurations of a prototype path during water splitting at $\theta = 228°$, including the initial molecular adsorption, the transition state, and dissociated products. In the final state, the hydrogen atom is bonded to the gold cluster and the OH bonds to the MgO substrate. Bader charge analysis shows that the H product is almost neutral, with $-0.04e$ charges, whereas the OH fragment has a net charge of $-0.85e$. The former is radically different from that for water dissociation on bare MgO, which produces a H charged by $+0.6e$ [28, 29].

Figure 5(b) shows the calculated activation energy (E_b) for water dissociation as a function of θ. The barrier varies dramatically between 0.85 ~ 1.33 eV and is highest at $\theta \approx 180°$ and lowest at $\theta \approx 250°$. This barrier is drastically reduced from that for the dissociation of gaseous water molecules (5 eV) and is close to the ideal value of 0.5–0.7 eV for efficient water splitting at near-ambient temperatures, although reaction rates may differ significantly. Because the OH group of the dissociated state is relatively far away from the gold cluster in all configurations, the energy change caused by OH group displacement is roughly constant, at about 0.33 ~ 0.44 eV, for different adsorption sites. Therefore the angular variation of energy barriers is mainly determined by the interaction between the dissociated H atom and the QWS in the transition state.

To illustrate this interaction in more detail, figure 5(c) shows the binding energy of an H atom, relative to isolated H and supported Au_8, as a function of θ, which indeed follows angular dependence similar to that of the dissociation barrier, as shown in figure 5(b). The binding energy of the H atom is almost identical to half the H–H bond energy (4.5 eV), facilitating H_2 release. It also shows a larger variation, ~0.4–0.6 eV, than that for water. The angular dependence is in excellent agreement with the charge density distribution of the QWS3 state shown in figure 5(d), where the maxima of the barrier and binding energy correspond to the antinodes at $\theta \approx 90°$ and 270° (and an additional smaller antinode at $\theta \approx 0°$). From figure 5, it is clear that the coupling between the H atom and QWS3 dominates the interaction between the gold cluster and the transition state, and thus modulates the energy barrier for water dissociation. Detailed analysis shows that the energy barrier is linearly dependent on the binding energy of H on Au_8, a nice demonstration of the Bronsted–Evans–Polonyi principle. Together with insights gained into the water–QWS2 quantum interaction, we expect that water splitting can be optimized on adsorption sites where wavefunction nodes of QWS2 meet QWS3 lobes with large overlap, such that H binding is drastically enhanced and simultaneously water adsorption is slightly destabilized to further reduce their energy difference, the reaction barrier. We find $\theta \approx 90°$ and 270° to be such optimal sites.

It is interesting to note that the dissociation barrier is essentially modulated by QWS3 rather than QWS2 as for molecular water adsorption. The different trends in water adsorption energies and dissociation barriers result from additional charge transfer from silver substrate at the transition state and the dissociated state, which makes QWS3 occupied and responsible for changes in H binding energetics during water splitting. Our Bader

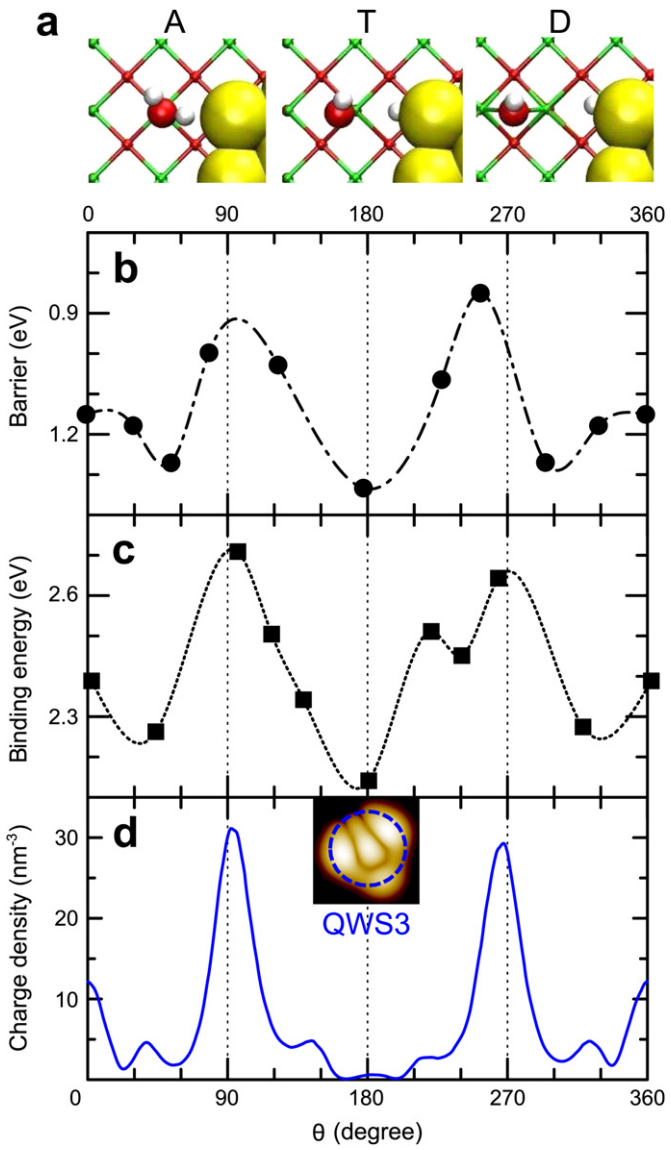

Figure 5. (a) Typical path for water dissociation starting from molecular adsorption of water (A) to the transition state of dissociation (T) to dissociated adsorption (D). (b) Water dissociation barriers and (c) H atom binding energies as a function of orientation angle. (d) Angular distribution of charge density of QW3 in the selected edge region. The inset shows the shape of QW3 and the edge zone.

charge analysis shows that an additional $0.6e \sim 1.4e$, approximately, are transferred from silver substrate to adsorbates during water dissociation. The LDOS analysis suggests that QWS3 shows a large downward shift of energy by about 1∼2 eV. We also found that this energy shift is the largest at $\theta = 90°$ and 270° (figure 3(a)), which further confirms that the dissociation barrier is modulated by the interaction between the H atom and QWS3.

Since molecule–QWS interaction is orientation dependent and state-selective, new rules might emerge for catalysis. For instance, conventional wisdom says that under coordinated metal atoms are often more reactive. However, in the present case where global QWSs dominate the adsorbate–metal interaction, we found no correlation between the local coordination number (CN) and reactivity: the apex gold atom with the closest water–Au distance and lowest CN = 2 is the most inert to water binding (energy 0.58 eV), whereas the edge gold atom with a large CN = 4 binds water most strongly (0.80 eV). Gold atoms with the same CN = 3 can have either the largest or smallest water binding energy, depending on global electronic features of QWSs. As a result, catalytic activity is strongly modulated by the orbit degree of freedom, where reaction rates at sites with the same lateral adsorbate–catalyst separation but different orientation can differ by five to seven orders of magnitude. One might use these advantages to improve catalytic activities by changing QWS occupation or by blocking unwanted sites by other adsorbates [10]. This conclusion is generic to other clusters supporting QWSs such as Au_{14} [16].

Our results reveal the mechanism of orbital-dependent modulation of catalytic activity using the QWS of a gold cluster supported on MgO thin films. The electronic interaction between water and the QWS is modulated by the symmetry and angular distribution of the frontier orbitals of the quantum well states and is state dependent. These findings provide new insights into understanding the catalytic activity of gold clusters and potential ways to utilize the new orbital degree of freedom for tuning the water splitting reaction.

Acknowledgments

We acknowledge partial financial support from MOST (grant 2012CB921403) and NSFC (grants 11222431 and 11290164), and the hundred-talent program of CAS. S G acknowledges support from VR and CSRC of China.

References

[1] Haruta M, Kobayashi T, Sano H and Yamada N 1987 *Chem. Lett.* **405**
[2] Yoon B, Hakkinen H, Landman U, Worz A S, Antonietti J-M, Abbet S, Judai K and Heiz U 2005 *Science* **307** 403
[3] Arenz M, Landman U and Heiz U 2006 *Chem. Phys. Chem.* **9** 1871
[4] Hutchings G J and Haruta M 2005 *Appl. Catal.* A **291** 2
[5] Hutchings G J 1985 *J. Catal.* **96** 292
[6] Nkosi B, Adams M D, Coville N J and Hutchings G J 1991 *J. Catal.* **128** 378
[7] Boccuzzia F, Chiorinoa A, Manzolia M, Andreevab D and Tabakovab T 1999 *J. Catal.* **188** 176
[8] Idrobo J C, Walkosz W, Yip S F, Öğüt S, Wang J and Jellinek J 2007 *Phys. Rev.* B **76** 205422
[9] Ferrighi L, Hammer B and Madsen G K H 2005 *J. Am. Chem. Soc.* **131** 10605
[10] Ding Z and Meng S 2012 *Phys. Rev.* B **86** 045455
[11] Yoon B, Koskinen P, Huber B, Kostko O, Issendorff B V, Häkkinen H, Moseler M and Landman U 2007 *Chem. Phys. Chem.* **8** 157
[12] Shao N, Huang W, Gao Y, Wang L M, Li X, Wang L S and Zeng X C 2010 *J. Am. Chem. Soc.* **132** 6596
[13] Gao Y, Shao N, Pei Y, Chen Z and Zeng X C 2011 *ACS Nano* **5** 7818
[14] Ricci D, Bongiorno A, Pacchioni G and Landman U 2006 *Phys. Rev. Lett.* **97** 036106
[15] Sterrer M, Risse T, Heyde M and Freund H-J 2007 *Phys. Rev. Lett.* **98** 206103
[16] Lin X, Nilius N, Freund H J, Walter M, Frondelius P, Honkala K and Hakkinen H 2009 *Phys. Rev. Lett.* **102** 206801
[17] Liu K and Gao S W 2012 *J. Phys. Chem.* C **116** 17613
[18] Sanchez A, Abbet S, Heiz U, Schneider W D, Ha1kkinen H, Barnett R N and Landman U 1999 *J. Phys. Chem.* A **103** 9573
[19] Hermann K, Bagus P S and Nelin C J 1987 *Phys. Rev.* B **35** 9467
[20] Kohn W and Sham L J 1965 *Phys. Rev.* **140** A1133
[21] Kresse G and Hafner J 1993 *Phys. Rev.* B **47** 558
[22] Vanderbilt D 1990 *Phys. Rev.* B **41** 7892
[23] Blöchl P E 1994 *Phys. Rev.* B **50** 17953
[24] Perdew J P, Burke K and Ernzerhof M 1996 *Phys. Rev. Lett.* **77** 3865
[25] Giordano L, Goniakowski J and Pacchioni G 2003 *Phys. Rev.* B **67** 045410
[26] Henkelman G, Uberuaga B P and Jónsson H 2000 *J. Chem. Phys.* **113** 9901
[27] Hu X L, Carrasco J, Klimeš J and Michaelides A 2011 *Phys. Chem. Chem. Phys.* **13** 12447
[28] Shin H-J, Jung J, Motobayashi K, Yanagisawa S, Morikawa Y, Kim Y and Kawai M 2010 *Nat. Mater.* **9** 442
[29] Jung J, Shin H-J, Kim Y and Kawai M 2010 *Phys. Rev.* B **82** 085413